https://doi.org/10.1016/j.ceramint.2021.05.273

Fabrication of in-situ Ti(C,N) phase toughened Al_2O_3 based ceramics from natural bauxite

Ziyan Li [1], Lvping Fu [1,2,3] *, Huazhi Gu [1], Siu Wing Or [2] *, Ao Huang [1], Renxiang Lv [3]

[1] The State Key Laboratory of Refractories and Metallurgy, Wuhan University of Science and Technology, Wuhan 430081, China

[2] Department of Electrical Engineering, The Hong Kong Polytechnic University, Hung Hom, Kowloon, Hong Kong

[3] Jinan Ludong Refractories Co., Ltd., Jinan 250109, China

*Corresponding author

Abstract

Al_2O_3-Ti(C,N) ceramics were fabricated via carbothermal reduction nitridation method with high-titania special-grade bauxite as the raw material. The formation mechanism of in-situ Ti(C,N) phase and its effect on the properties of materials are discussed. After nitrided at 1700 °C, Ti(C,N) phase could be formed in-situ with appropriate C/TiO_2 molar ratio. Due to the residual stress field formed by Ti(C,N) particles, the path of crack propagation is changed, leading to the crack deflection and pinning. Therefore, the mechanical properties of the materials are improved by forming in-situ Ti(C,N) phase. With a C/TiO_2 molar ratio of 2.2 and nitridation temperature of 1700 °C, Al_2O_3-Ti(C,N) ceramic with a hardness of 13.9 GPa, a fracture toughness of 8.28 MPa $m^{1/2}$ and a flexural strength of 387 MPa could be fabricated.

Key words: Ti(C,N); toughening; Al_2O_3 based ceramic; bauxite; mechanical properties

1 Introduction

Because of the low cost, good chemical stability, excellent mechanical strength and outstanding high-temperature thermodynamic stability of alumina ceramics, they have been proverbially employed as armor systems, refractory crucibles, coatings, thermal insulators, and dental prostheses [1,2]. However, the application range of alumina ceramics has been restricted by its unsatisfied fracture toughness [3]. Therefore, numerous studies have been conducted for improving the fracture toughness of alumina ceramics. Generally, two main approaches are currently used in the reported works:

(i) Microstructure refinement. The fracture toughness of alumina ceramics could be enhanced by adjusting the shape or size of grains and the amounts of defects [4,5]. For example, toughness enhancement of alumina ceramics could be achieved by elongated or coarse grains, decreasing the grain size and avoiding the formation of defects.

(ii) Introducing some additives or second phases to form composites. By adding metals, intermetallics, ceramic particles, whiskers or fibres, the fracture toughness could be enhanced due to plastic deformation, crack bridging and crack deflection toughening mechanism [6].

In general, composite formulations create better performance improvements than microstructure refinement. SiC, Si_3N_4, B_4C, Ti(C,N) are the popular second phase additives in alumina based ceramics [7-12]. Among that, Ti(C,N) ceramic is expected to exhibit superior toughness, hardness, wear resistance and thermal shock resistance, therefore, is now very attractive for the reinforcement of alumina. Using gas pressure sintering, Al_2O_3-Ti(C,N) composite was obtained by Yang et al. [13], the composite exhibited a hardness and fracture

toughness of 19.6 GPa and 5.82 MPa $m^{1/2}$, respectively. Al_2O_3-Ti(C,N)-ZrO_2 nanocomposites with a hardness of 21 GPa and toughness of 5.5 MPa $m^{1/2}$ were developed by Chakravarty et al. [14]. However, the Al_2O_3-Ti(C,N) composites were usually prepared by adding Ti(C,N) powder into alumina powder. The cost of Ti(C,N) powder is typically very high. And more importantly, the densification of Ti(C,N) particles is very difficult, requiring pressure sintering or SPS to achieve sintering densification [15,16].

The sintering difficulty of Al_2O_3-Ti(C,N) composites might be avoided by forming in-situ Ti(C,N) in alumina system. It is well recognized that Ti(C,N) phase could be obtained from carbothermal reduction nitridation of TiO_2 [17,18]. Using anatase TiO_2 and electrode graphite powder as raw materials, Ti(C,N) powder was synthesised by Yang et al. through carbothermal reduction-nitridation at 1380 °C [17]. High-titania special-grade bauxite is a widespread natural raw material, whose main chemical composition is Al_2O_3 and TiO_2. By adopting carbothermal reduction nitridation method, the TiO_2 in high-titania special-grade bauxite would transform into in-situ Ti(C,N) phase. Consequently, in this work, Al_2O_3-Ti(C,N) ceramics were fabricated with high-titania special-grade bauxite as the raw material. The formation mechanism of in-situ Ti(C,N) phase and its effect on the properties of ceramics are investigated.

2. Experimental

2.1 Starting materials

High-titania special-grade bauxite and carbon black were selected as the starting materials. Carbon black is supplied by Wuhan Kebon New Materials Co., Ltd., Wuhan, China.

The carbon content of nano carbon black is ≥99.5 wt%, and the average particle size is 30 nm. The chemical compositions of high-titania special-grade bauxite are shown in Tables 1. Besides small amounts of SiO_2, Fe_2O_3 and CaO, the high-titania special-grade bauxite consists mainly of alumina and titania. The total content of Al_2O_3 and TiO_2 is up to 97.83 wt%. As provided in Fig. 1 (a), the particle size of bauxite showed multi-peak distribution, and the median particle diameter was 3.44 μm. As for the TG and DSC traces of bauxite given in Fig. 1 (b), a weight loss of approximately 16 % was measured from 25 °C to 1500 °C. Due to the eliminating of immobilized water in diaspore and kaolinite, a large weight-loss was detected in the temperature range of 450–550 °C. One endothermic peak, around 505.1 °C, was observed, which is caused by the water removal of weight-loss diaspore and kaolinite.

Table 1. Chemical compositions of high-titania special-grade bauxite

Raw materials	Chemical compositions/wt%								
	Al_2O_3	MgO	SiO_2	Fe_2O_3	K_2O	Na_2O	TiO_2	CaO	IL
Original composition	79.71	0.11	0.72	0.39	0.01	0.01	3.99	0.37	14.45
Composition without IL	93.17	0.13	0.84	0.46	0.01	0.01	4.66	0.43	-

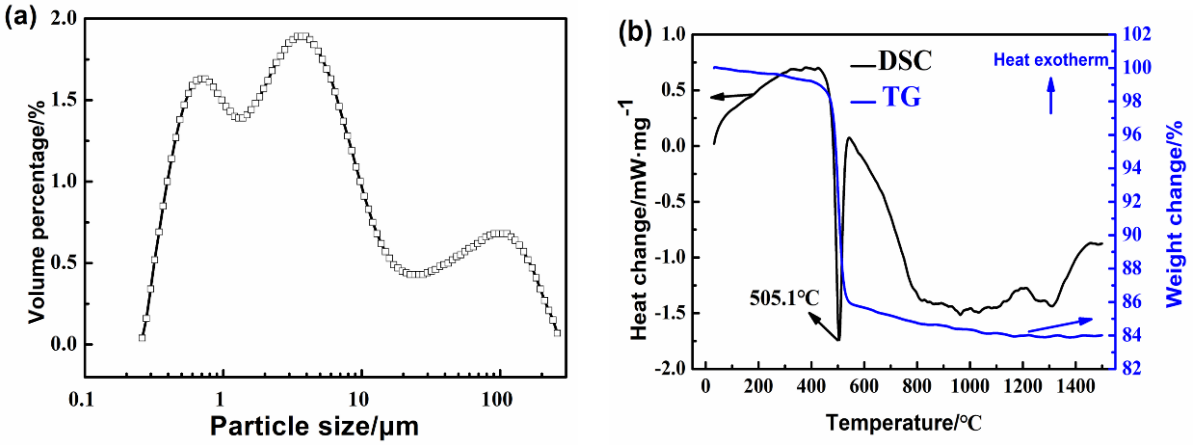

Fig. 1. (a) Particle size distribution and (b) thermal analysis results of bauxite

2.2 Sample preparation

The theoretical reaction equation for the carbothermic reduction nitriding of TiO_2 is shown in Equation (1). Depending on the element ratios in target product, the molar ratio of C/TiO_2 is usually in the range from 2 to 3. Theoretically, when the C/TiO_2 molar ratio (CTMR) is 2, the reaction product would be TiN phase, and TiC would be obtained when the CTMR is 3.

$$TiO_2 + (3-x)C + \frac{x}{2}N_2 \rightarrow Ti(C_{1-x}N_x) + 2CO \quad (1)$$

In this study, since the target product in this experiment is Ti(C,N) phase, the CTMRs in samples were set as 2, 2.2, 2.5 and 2.8, respectively. High-titania special-grade bauxite and nano carbon black were wet-milled for 30 minutes to produce slurry. The slurry was dried at 110 °C for 24 hours and followed by 200 mesh sieving. With 1 wt% polyvinyl alcohol as the binder, the sieved powder was then uniaxially pressed into green bodies at 150 MPa. After being dried at 110 °C for 24 hours, the green bodies were heated at 1700 °C for 3 hours in a nitrogen-atmosphere electric furnace.

2.3 Characterisation

The dimensions of samples before and after sintering were measured to calculate the linear shrinkage. The bulk densities and open porosities were determined based on the Archimedes' method. The true densities of sintered samples were measured by a helium pycnometer analyzer using 325 mesh-sieved powder.

Phase identification was carried out by means of an X-ray diffractometer. The microstructure of specimen was analyzed by a scanning electron microscope and their element distributions were tested with an attached energy dispersive X-ray spectrometer.

Three-point flexural strength test was carried out on the samples with a span of 30 mm.

The Vickers hardness of sintered samples were tested on the polished surfaces using Vickers hardness tester (HV-50A, Laizhou Huayin Testing Instrument Co., Ltd., China) equipped with a diamond pyramid indenter. The tested load was 5 kg and the loading duration is 10 s, according to Echeberria and Yu's works [19,20]. As shown in Fig. 2, the Vickers hardness and fracture toughness of samples then could be calculated using the following equations:

$$Hv = \frac{1.8544P}{102d^2} \tag{2}$$

$$K_{IC} = 0.028 \times Hv^{0.5} \times E^{0.5} \times a^2 \times c^{-1.5} \tag{3}$$

$$E = E_1V_1 + E_2V_2 + \cdots \tag{4}$$

where H_v is the Vickers hardness (GPa); P is the loading load (kg); d is the average value of d_1 and d_2 (mm); K_{IC} is the fracture toughness (MPa $m^{1/2}$); E is the elastic modulus (MPa); a is half length of d; c is the crack half-length (m); E_1 and E_2 are the elastic modulus of each component in the sample (MPa); V_1 and V_2 are the volume fraction of each component in the sample.

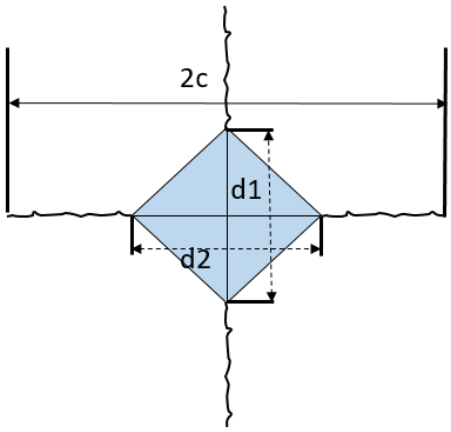

Fig. 2. Schematic diagram of indentation and cracks caused by Vickers

3. Results

3.1 Phase compositions

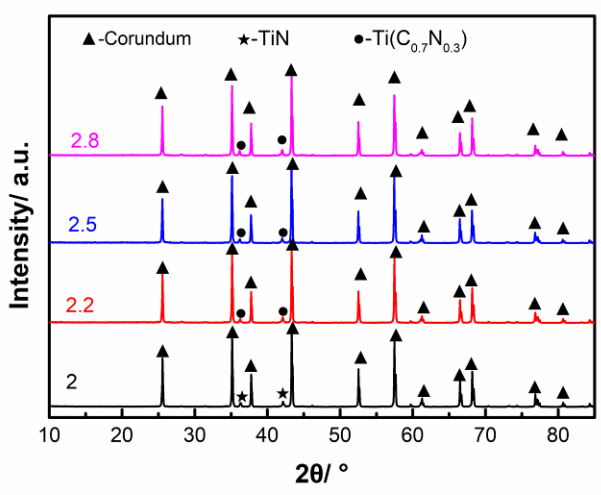

Fig. 3. Phase compositions of nitrided samples with different CTMRs

The XRD patterns of nitrided samples with various CTMRs are provided in Fig. 3. After nitridation, the sample with a CTMR of 2 is mainly composed of corundum and TiN phases, indicating the TiO_2 component in bauxite reacts with nitrogen to generate TiN phase. With the increased introduction of carbon, the phase of TiN was transformed into Ti(C,N), the peak of TiN phase disappeared and the peak of $Ti(C_{0.7}N_{0.3})$ was detected. Moreover, the peak intensity of $Ti(C_{0.7}N_{0.3})$ phase increased with increasing CTMR.

As provided in Table 2, the XRD patterns were refined using a Celref calculation software (Beta Version 2000, Grenoble INP, France) to determine the lattice constants of $Ti(C_{0.7}N_{0.3})$ phase in different samples. The lattice constant of $Ti(C_{0.7}N_{0.3})$ phase increased with increasing CTMR. This may be attributed to the increased solid solution of C into $Ti(C_{0.7}N_{0.3})$ phase. Since the C atom has a greater atomic radius than that of N atom, the solid solution of C would lead to increased lattice constant of $Ti(C_{0.7}N_{0.3})$ phase.

Table 2. Lattice parameters of Ti($C_{0.7}N_{0.3}$) phases in various samples

CTMR	a/ Å	b/ Å	c/ Å
2.2	4.2927	4.2927	4.2927
2.5	4.2947	4.2947	4.2947
2.8	4.2953	4.2953	4.2953

3.2 Microstructure

SEM microphotographs of the polished surfaces of nitrided samples with different CTMRs are shown in Fig. 4. In accordance with the XRD results, for the sample with a CTMR of 2, the TiN phase was formed in situ after nitridation. The TiN phase, bright points in Fig. 4 (a), was uniformly dispersed in the sample. As given in Table 3, the energy spectrum results suggested that a small amount of O element was dissolved in the TiN phase. Several pores could be found between the grains.

With respect to the specimen with a CTMR of 2.2, it showed a lower porosity and increased density (Fig. 4 (b)). As shown in Table 3, the Ti element mainly existed in the form of Ti(C,N) phase. With the CTMR further increased to 2.5, the content of C in the Ti(C,N) phase was accordingly raised. Nevertheless, the porosity of the sample increased instead (Fig. 4 (c)), which may be caused by the densification difficulty of Ti(C,N) material. Fig. 4 (e) provides the mapping scanning result of the area in the red dotted square in the upper right corner of Fig. 4 (c). The distribution of Ti, C and N elements is relatively overlapping, indicating the generation of Ti(C,N) phase. With the CTMR further increased to 2.8, the content of C in the Ti(C,N) phase further augmented while sample compactness further decreased (Fig. 4 (d)).

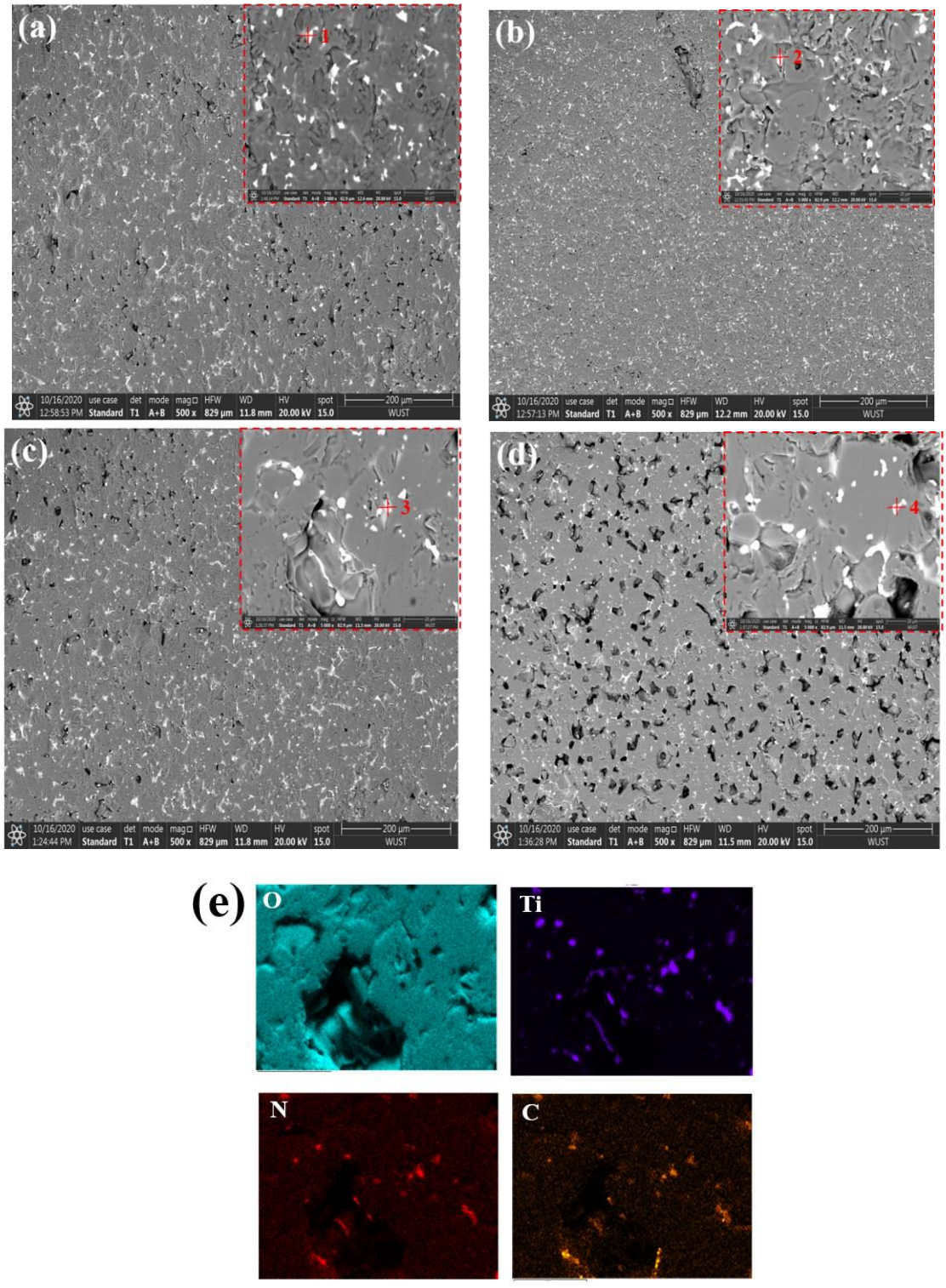

Fig. 4. SEM images of polished surfaces of samples with different CTMRs: (a) 2, (b) 2.2, (c) 2.5, (c) 2.8; (e) element distribution of selected area in the top right corner of figure (c)

Table 3. Energy dispersive analyses of various samples

Points	Ti/ wt%	C/ wt%	N/ wt%	O/ wt%	Possible phase
1	81.7	0.3	16.9	1.1	TiN
2	81.6	6.1	11..	0.8	Ti(C,N)
3	80.1	8.9	10.1	0.8	Ti(C,N)
4	76.2	11.0	11.9	0.8	Ti(C,N)

3.3 Sintering properties

Sintering properties of the samples nitrided at 1700 °C with various CTMRs are shown in Table 4. For the sample with a CTMR of 2, it has a relative density of 91.3 %, while the total porosity was 8.7 %.

The transformation of TiN into Ti(C,N) phase may affect the densification behavior of materials from two aspects. On the one hand, since the C atom has a greater atomic radius than that of N atom, with the solid solution of C into TiN, it has been reported that the Ti(C,N) phase possesses a lower theoretical density than that of TiN [21]. Therefore, a certain volume expansion would be occurred during the transformation, which may fill in the pores, resulting in a lower porosity. On the other hand, by comparing the effects of TiN, TiC and Ti(C,N) additions on the properties of alumina-based ceramics, several published works have already pointed out the Ti(C,N)-added ceramic showed the worst sinterability, when being compared to ceramics containing addition of TiN or TiC [22,23]. Thus, in this case, an excessive content of Ti(C,N) phase might lead to poor densification.

When the CTMR increased to 2.2, the TiN phase in the sample transformed into Ti(C,N) phase, accompanying with a certain volume expansion, which may fill in the pores. Therefore,

the bulk density and linear shrinkage of the sample increased, while the total porosity decreased. However, with the CTMR further increased to 2.5 and 2.8, the amount of generated Ti(C,N) phase consequently increased. The impact caused by poor sinterability of Ti(C,N) phase would be more significant. Therefore, the linear shrinkage and bulk density reduced, while the total porosity increased.

Table 4. Sintering properties of samples with different CTMRs

C/TiO_2 molar ratio	Linear shrinkage (%)	Bulk density (g/cm^3)	True density (g/cm^3)	Total porosity (%)
2	20.9	3.46	3.79	8.7
2.2	21.8	3.54	3.81	7.2
2.5	21.1	3.48	3.81	8.7
2.8	20.4	3.34	3.82	12.7

3.4 Mechanical properties

Fig. 5 provides the mechanical properties of various samples. With the introduction of carbon, the mechanical properties of nitrided samples showed a trend of increased initially and then decreased. With respect to the sample with a CTMR of 2.2, the TiN phase transformed into Ti(C,N) phase, leading to raised density and decreased porosity (Table 4). Since the Ti(C,N) phase possesses a better hardness than TiN phase [24,25], the hardness of the samples was improved. Although it has been pointed out that the fracture toughness of Ti(C,N) phase is slightly lower than that of TiN phase [24,25], the toughness and strength of the sample are increased when the CTMR increased to 2.2. This may be due to better sintering degree and lower porosity in the sample.

With CTMR further increased to 2.5 and 2.8, the relative density of the samples decreased and the porosity increased, which has a negative effect the mechanical properties of the materials.

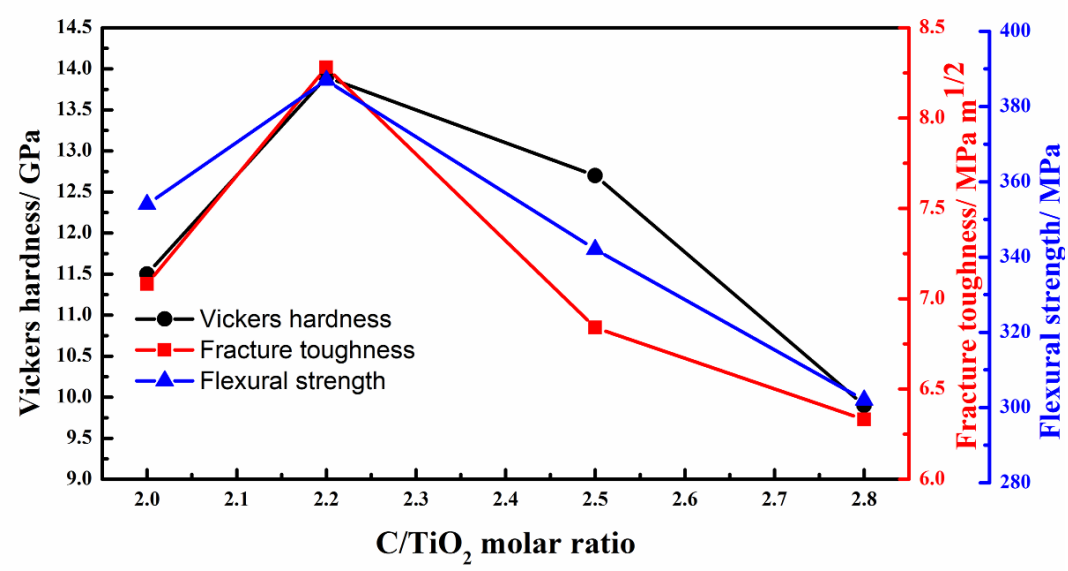

Fig. 5. Mechanical properties of samples with different CTMRs

4. Discussion

4.1 Formation of Ti(C,N) phase

In order to understand the formation process of Ti(C,N) phase, thermodynamic calculations were carried out to predict the equilibrium phase by using the 'Equilibrium' module of FactSage 6.4. The predicted equilibrium solid phases in TiO_2-C-N_2 system at different CTMRs are shown in Fig. 6.

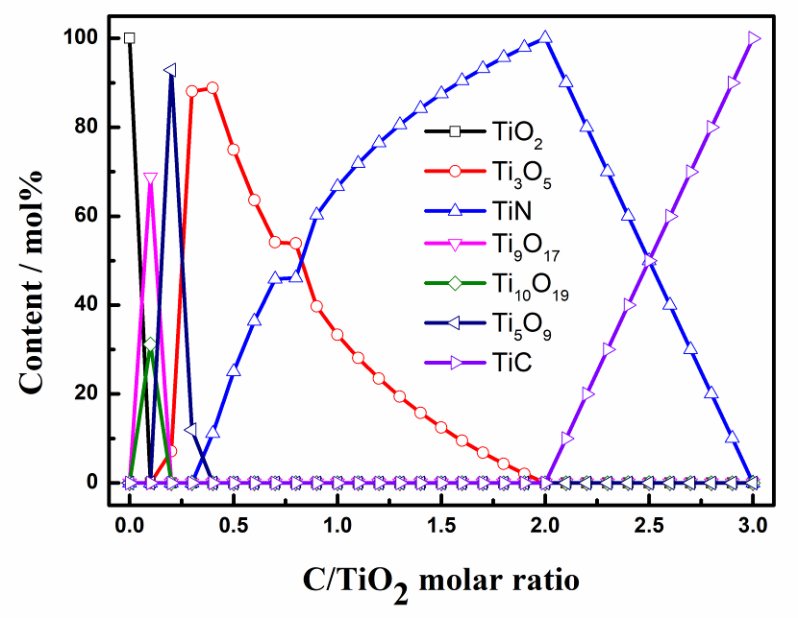

Fig. 6. Predicted solid phase compositions in TiO_2-C-N_2 system with different CTMRs at 1700 °C

It should be pointed out that, since Ti(C,N) phase is the solid solution of TiC and TiN, the Ti(C,N) phase was represented in the form of TiC and TiN during the thermodynamic calculations.

When the CTMR is equal to 0, the only solid phase in TiO_2-C-N_2 system is TiO_2, indicating the reaction between TiO_2 and will not occur without the involvement of carbon. With the CTMR increases to 0.1, the TiO_2 disappears and transforms into Ti_9O_{17} and $Ti_{10}O_{19}$. With the CTMR further increases to 0.2 and 0.3, Ti_9O_{17} and $Ti_{10}O_{19}$ has not been found, they all converte to Ti_3O_5 and Ti_5O_9. When the CTMR reaches 0.4, TiN phase appears for the first time, only Ti_3O_5 and TiN are generated in the TiO_2-C-N_2 system. For the CTMR in the range from 0.4 to 1.9, the type of solid phases in system remains unchanged, consisting of Ti_3O_5 and TiN. With the increasing CTMR, the content of Ti_3O_5 decreases while the TiN content

increases. When the CTMR increases to 2, the Ti_3O_5 phase disappears and TiN phase is the only solid phase. With the CTMR further increases, TiC phase begins to appear in the system. With the increase of CTMR, the content of TiC in equilibrium phase increases and the content of TiN decreases.

A large number of studies have been carried out on the behavior of carbothermal reduction nitridation of TiO_2. The reaction in this work was carried out in a closed system in an atmosphere furnace, therefore it is considered that the carbothermal reduction reaction in the early stage occurred by the solid-solid reaction between TiO_2 and C. According to our experimental results and thermodynamic calculations, the formation process of Ti(C,N) phase could be roughly classified into the following three stages.

(1) The first stage, the carbothermal reduction of TiO_2 occurs, and the products are series of intermediate titanium oxides, Ti_nO_{2n-1}.

$$nTiO_2 + C \rightarrow Ti_nO_{2n-1} + CO \quad (5)$$

$$3Ti_nO_{2n-1} + (n-3)C \rightarrow nTi_3O_5 + (n-3)CO \quad (6)$$

As shown in Equation (6), at a lower temperature, TiO_2 will undergo a reduction reaction with C to form the intermediate titanium oxide, Ti_nO_{2n-1}. The intermediate titanium oxide Ti_nO_{2n-1} is easily to be converted into Ti_5O_9, $Ti_{10}O_{19}$, Ti_9O_{17} and other intermediate titanium oxides. Among which, Ti_3O_5 is the most stable intermediate titanium oxide in N_2 atmosphere.

(2) In the second stage, the intermediate titanium oxides disappears and Ti(C,N,O) phase is formed.

$$Ti_3O_5 + (5-3z_1)C + \frac{3y_1}{2}N_2 \rightarrow 3Ti(N_{y1}, O_{z1}) + (5-3z_1)CO \quad (7)$$

$$Ti_3O_5 + (5+3x_1-3z_2)C \rightarrow 3Ti(C_{x1}, O_{z2}) + (5-3z_2)CO \quad (8)$$

$$Ti(N_{y1}, O_{z1}) + Ti(C_{x1}, O_{z2}) \rightarrow Ti(C_{x2}, N_{y2}, O_{z3}) \quad (9)$$

With the increase of temperature, N_2 begins to participate in the reaction, and Ti_3O_5 reacts with N_2 and C to form Ti(N,O) and Ti(C,O), respectively. Through the reaction of Equation (9), Ti(C,N,O) phase is generated form the reaction between Ti(N,O) and Ti(C,O) phase.

(3) In the third stage, C atoms replace O in Ti(C,N,O) phase to gengrate Ti(C,N) phase.

$$Ti(C_{x2}, N_{y2}, O_{z3}) + C \rightarrow Ti(C_{x3}, N_{y3}) + CO \quad (10)$$

As the reaction continues, C in the reactants replaces O in the Ti(C,N,O) phase, transforming the Ti(C,N,O) phase into Ti(C,N) phase.

4.2 Effect of in-situ Ti(C,N) on mechanical properties of materials

Aiming to understand the formation of in-situ Ti(C,N) phase on the properties of materials, bauxite was sintered in air to set as the control specimen, and the properties of control specimen were listed in Table 5. For the sample with a CTMR of 2.2 and 2.5, although they exhibited higher porosities than that of the control specimen, the mechanical properties were surprisingly improved. These results indicated the formation of in-situ Ti(C,N) has a positive impact on the mechanical properties of samples. With the CTMR further increased to 2.8, the sample showed lower hardness and flexural strength due to a too high porosity.

Therefore, the effect of in-situ Ti(C,N) on properties of materials are discussed in the following.

Table 5. Properties of the control specimen

Bulk density (g/cm^3)	Total porosity (%)	Vickers hardness (GPa)	Fracture toughness (MPa $m^{1/2}$)	Flexural strength (MPa)
3.71	2.8	11.2	6.05	312

Owing to the difference in thermal expansion coefficient and elastic modulus between Ti(C,N) and Al_2O_3, significant residual internal stress would be produced between Ti(C,N) particles and Al_2O_3 matrix.

The stress P on the second phase particle can be calculated by using Equation (11) [26]:

$$P = \frac{2\Delta\alpha\Delta T E_m E_p}{E_p(1+\nu_m) + 2E_m(1-2\nu_p)} \tag{11}$$

where $\Delta\alpha$ is the thermal expansion coefficient difference between the second phase particles and matrix; ΔT is the temperature difference during the cooling stage; E_m, ν_m and E_p,ν_p are the elastic modulus and Poisson's ratio of the matrix and the second phase particles, respectively.

This internal stress will form a radial tensile stress σ_r and the circumferential tensile stress σ_t in the matrix [26]:

$$\sigma_{\mathrm{r}} = -P\left(\frac{R}{r}\right)^3 \tag{12}$$

$$\sigma_{\mathrm{t}} = \frac{P}{2}\left(\frac{R}{r}\right)^3 \tag{13}$$

where R is the radius of inclusion; r is the distance.

According to Equations (12) and (13), the magnitude of residual stress is related to the distance between this point and the center of inclusion particle.

The elastic strain energies stored in the second phase particle and its surrounding matrix can be obtained [26]:

$$U_p = 2\pi \frac{P^2(1-2\nu_p)}{E_p} R^3 \tag{14}$$

$$U_m = \pi \frac{P^2(1+\nu_m)}{E_m} R^3 \tag{15}$$

The linear expansion coefficient of Ti(C,N) is 8.35×10^{-6}/°C, while that of Al_2O_3 is 8.237×10^{-6}/°C [27]. According to Equation (11), $\Delta\alpha$ and P are greater than 0. Based on Equations (12) and (13), a tensile stress will be generated inside the second phase particle, and radial tensile stress and tangential compressive stress will be generated in the surrounding matrix.

As shown in Fig. 7, cracks always propagate along the weak link of the stress field, parallel to the compressive stress and perpendicular to the tensile stress. When the cracks extend around the second phase particle, they will propagate towards the second phase particle. Since the closer to the second phase particle, the greater the residual stress, the cracks will be pinned to or deflected towards the second phase particle.

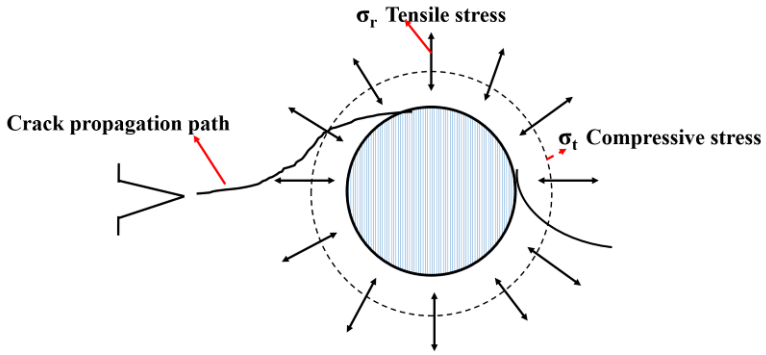

Fig. 7 Effect of inclusion particle residual stress on the crack propagation path

According to Taya's model, the increased fracture toughness enhanced by the residual stress, Δ_{IC}, could be described using Equations (16)-(17):

$$\Delta_{IC} = 2P\sqrt{\frac{2(\lambda - d)}{\pi}} \tag{16}$$

$$\lambda = \frac{1.085d}{\sqrt{f_p}} \tag{17}$$

where λ is the center distance between inclusions; d is the diameter of inclusion; f_p is the volume fraction of the inclusion.

In order to give a quantitative description on the mechanical properties change of samples, the residual stress in the control specimen and the Al_2O_3-Ti(C,N) sample with a CTMR of 2.2 were calculated using Equation (11). The parameters during the calculation are listed in Table 6.

Table 6. The parameters during the calculation of residual stress

Materials	Linear expansion coefficient ($\times 10^{-6}$/°C)	Elastic modulus (GPa)	Poisson's ratio
Al_2O_3	8.237 [27]	465 [29]	0.234 [29]
Al_2TiO_5	1.5 [30]	250 [31]	0.25 [31]
Ti(C,N)	8.35 [27]	570 [29]	0.19 [29]

By introducing the parameters in Table 6 into Equations (16)-(17), the value of Δ_{IC} was calculated to be 2.408 MPa $m^{1/2}$, which is similar to the experimental results.

Fig. 8 shows the SEM photos presenting the effect of in-situ Ti(C,N) particles on the crack propagation path, in which the bright-colored particles are Ti(C,N) particles. Owing to the residual stress field formed by Ti(C,N) particles, the path of crack propagation is changed,

leading to the crack deflection and pinning. The energy of crack propagation is absorbed and consumed, the driving force of forward propagation is reduced, therefore, the fracture toughness is improved. At the same time, due to the advantages of high hardness (over 23 GPa) and high elastic modulus (over 570 GPa) of Ti(C,N) particles [29,32], it acts as a reinforcement particle in the matrix of alumina, the hardness and flexural strength of the materials are also subsequently improved.

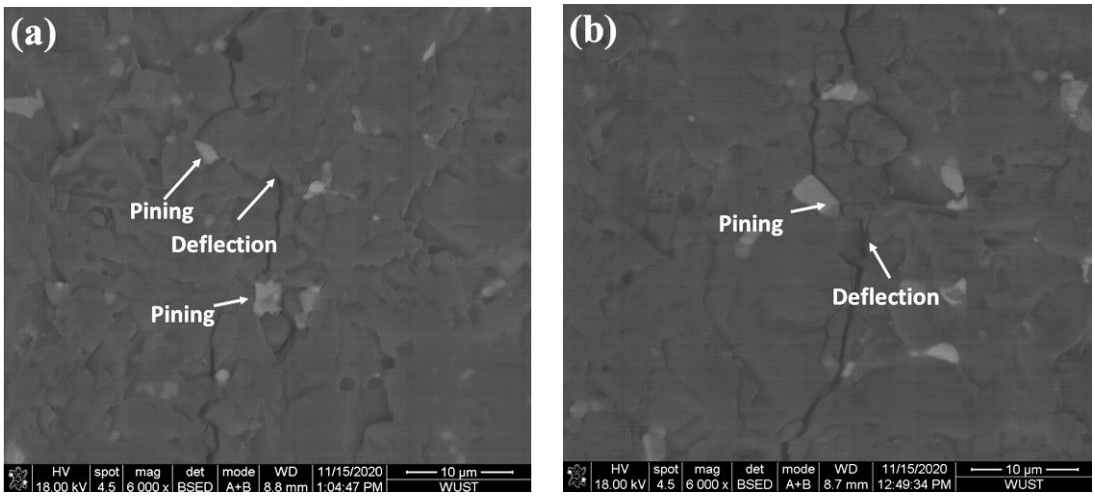

Fig. 8. Effect of in-situ Ti(C,N) particles on the crack propagation of samples

5. Conclusions

(1) After nitrided at 1700 °C, TiN phase was formed in situ in the sample with a CTMR of 2. With the CTMR increase to 2.2, the TiN phase in the sample transformed into Ti(C,N) phase, the bulk density and linear shrinkage increased, leading to improved mechanical properties. However, when CTMR is further increased to 2.5 and 2.8, the bulk density of the samples decreased, while the total porosity increased. Therefore, the mechanical properties of the samples degraded instead.

(2) Due to the residual stress field formed by Ti(C,N) particles, the path of crack propagation is changed, leading to the crack deflection and pinning. The energy of crack propagation is absorbed and consumed, and the driving force of forward propagation is reduced. Moreover, Ti(C,N) particles have the advantages of good hardness and high elastic modulus. Therefore, the materials are toughened by forming in-situ Ti(C,N) phase.

(3) With a CTMR of 2.2 and nitridation temperature of 1700 °C, alumina-Ti(C,N) ceramic with a bulk density of 3.54 g/cm^3, Vickers hardness of 13.9 GPa, fracture toughness of 8.28 MPa m$^{1/2}$ and flexural strength of 387 MPa could be fabricated.

Acknowledgements

This work is financially supported by the National Natural Science Foundation of China (Grant No. 51802231), the Hong Kong Scholars Program 2020 (Grant No. G-YZ4E/ XJ2020023), the China Postdoctoral Science Foundation (Grant No. 2017M622535), and the WUST National Defence Pre-research Foundation (Grant No. GF201905).

References

[1] M. Schwentenwein, J. Homa, Additive manufacturing of dense alumina ceramics, Int. J. Appl. Ceram. Tec. 12 (2015) 1-7. https://doi.org/10.1111/ijac.12319

[2] L.P. Fu, H.Z. Gu, A. Huang, Y.S. Zou, M.J. Zhang, Fabrication of lightweight alumina with nanoscale intracrystalline pores, J. Am. Ceram. Soc. 103 (3) (2020) 2262-2271. https://doi.org/10.1111/jace.16914

[3] O. L. Ighodaro, O.I. Okoli, Fracture Toughness Enhancement for Alumina Systems: A Review, Int. J. Appl. Ceram. Tec. 5 (2008) 313-323. https://doi.org/10.1111/j.1744-7402.2008.02224.x

[4] H. Manshor, S.M. Aris, A.Z. A. Azhar, E.C. Abdullah, Z.A. Ahmad, Effects of TiO_2

addition on the phase, mechanical properties, and microstructure of zirconia-toughened alumina ceramic composite, Ceram. Int. 41 (2015) 3961–3967. https://doi.org/10.1016/j.ceramint.2014.11.080

[5] J.J. Liu, B. Ren, Y.J. Lu, X.Q. Xi, Y.J. Li, K.L. Liu, J.L. Yang, Y. Huang, Novel design of elongated mullite reinforced highly porous alumina ceramics using carbonized rice husk as pore-forming agent, Ceram. Int. 45 (2019) 13964–13970. https://doi.org/10.1016/j.ceramint.2019.04.095

[6] I. Ahmad, M. Islam, H.S. Abdo, T. Subhani, K.A. Khalil, A.A. Almajid, B. Yazdani, Y.Q. Zhu, Toughening mechanisms and mechanical properties of graphene nanosheet-reinforced alumina, Mater. Des. 88 (2015) 1234–1243. https://doi.org/10.1016/j.matdes.2015.09.125

[7] B. Yazdani, Y.D. Xia, I. Ahmad, Y.Q. Zhu, Graphene and carbon nanotube (GNT)-reinforced alumina nanocomposites, J. Eur. Ceram. Soc. 35 (2015) 179–186. https://doi.org/10.1016/j.jeurceramsoc.2014.08.043

[8] Y. Yin, B.Y. Ma, C.B. Hu, G. Q. Liu, H.X. Li, C. Su, X.M. Ren, J.Y. Yu, Y.R. Zhang, J.K. Yu, Preparation and properties of porous SiC-Al_2O_3 ceramics using coal ash, Int. J. Appl. Ceram. Tec. 16 (2019) 23-31. https://doi.org/10.1111/ijac.13080

[9] X.M. Ren, B.Y. Ma, Y.R. Zhang, D.X. Li, Q. Zhu, L. Yuan, J.K. Yu, G.Q. Liu, H.X. Li, Effects of sintering temperature and V_2O_5 additive on the properties of SiC-Al_2O_3 ceramic foams, J. Alloy. Compd. 732 (2018) 716-724. https://doi.org/10.1016/j.jallcom.2017.10.170

[10] Z.L. Liu, C.J. Deng, C. Yu, X. Wang, J. Ding, H.X. Zhu, Molten salt synthesis and characterization of SiC whiskers containing coating on graphite for application in Al_2O_3-SiC-C castables, J. Alloy. Compd. 777 (2019) 26-33. https://doi.org/10.1016/j.jallcom.2018.09.107

[11] P. Tan, P. Wu, L. Gao, Y.D. Sui, Y.H. Jiang, Influence of Si_3N_4 content on the physical and

mechanical properties of zirconia-toughened alumina (ZTA) ceramic composites, Mater. Res. Express. 6 (2019) 065205. https://doi.org/10.1088/2053-1591/ab0e54

[12] R.Z. Liu, P. Chen, J.M. Wu, S. Chen, A.N. Chen, J.Y. Chen, S.S. Liu, Y.S. Shi, C.H. Li, Effects of B_4C addition on the microstructure and properties of porous alumina ceramics fabricated by direct selective laser sintering, Ceram. Int. 44 (2018) 19678–19685. https://doi.org/10.1016/j.ceramint.2018.07.220

[13] H.T. Yang, F.L. Shang, L. Gao, Microstructure and mechanical properties of gas pressure sintered Al_2O_3/TiCN composite, Ceram. Int. 33 (2007) 1521–1524. https://doi.org/10.1016/j.ceramint.2006.07.001

[14] D. Chakravarty, G. Sundararajan, Microstructure, mechanical properties and machining performance of spark plasma sintered Al_2O_3–ZrO_2–TiCN nanocomposites, J. Eur. Ceram. Soc. 33 (2013) 2597–2607. https://doi.org/10.1016/j.jeurceramsoc.2013.04.021

[15] G.H. Liu, R. Li, T.C. Yuan, M. Zhang, F.H. Zeng, Spark plasma sintering of pure TiCN: Densification mechanism, grain growth and mechanical properties, Int. J. Refract. Met. H. 66 (2017) 68–75. https://doi.org/10.1016/j.ijrmhm.2017.02.008

[16] R. Landfried, F. Kern, W. Burger, W. Leonhardt, R. Gadow, Development of electrical discharge machinable ZTA ceramics with 24 vol% of TiC, TiN, TiCN, TiB_2 and WC as electrically conductive phase, Int. J. Appl. Ceram. Tec. 10 (2013) 509-518. https://doi.org/10.1111/j.1744-7402.2012.02756.x

[17] Y.F. Yang, L.B. Ma, Z.H. Huang, M.X. Jiang, The effects of partial pressure of CO on the phase behaviour of synthesised Ti(C,N) through carbothermal reduction-nitridation at 1380 °C, Ceram. Int. 46 (2020) 19708–19712. https://doi.org/10.1016/j.ceramint.2020.04.167

[18] S.A. Rezan, G.Q. Zhang, O. Ostrovski, Effect of gas atmosphere on carbothermal reduction and nitridation of titanium dioxide, Metall. Mater. Trans. B. 43 (2012) 73-81.

https://doi.org/10.1007/s11663-011-9574-6

[19] J. Echeberria, N. Rodríguez, J. Vleugels, K. Vanmeensel, A. Reyes-Rojas, A. Garcia-Reyes, C. Domínguez-Rios, A. Aguilar-Elguézabal, M.H. Bocanegra-Bernal, Hard and tough carbon nanotube-reinforced zirconia-toughened alumina composites prepared by spark plasma sintering, Carbon. 50 (2012) 706-717. https://doi.org/10.1016/j.carbon.2011.09.031

[20] M.X. Yu, J.X. Zhang, X.G. Li, H.Q. Liang, H. Zhong, Y.S. Li, Y.S. Duan, D.L. Jiang, X.J. Liu, Z.R. Huang, Optimization of the tape casting process for development of high performance alumina ceramics, Ceram. Int. 41 (2015) 14845-14853. https://doi.org/10.1016/j.ceramint.2015.08.010

[21] M.X. Zhang, H.L. Yao, H.T. Wang, Q.Y. Chen, X.B. Bai, X.R. Zhao, Y.F. Fang, H. Xu, Q.T. Li, In situ Ti(C,N)-based cermets by reactive hot pressing: Reaction process, densification behavior and mechanical properties, Ceram. Int. 45 (2019) 1363-1369. https://doi.org/10.1016/j.ceramint.2018.07.270

[22] R. Landfried, F. Kern, W. Burger, W. Leonhardt, R. Gadow, Development of electrical discharge machinable ZTA ceramics with 24 vol% of TiC, TiN, TiCN, TiB_2 and WC as electrically conductive phase, Int. J. Appl. Ceram. Tec. 10 (2013) 509-518. https://doi.org/10.1111/j.1744-7402.2012.02756.x

[23] M. Szutkowska, S. Cygan, M. Podsiadło, J. Laszkiewicz-Łukasik, J. Cyboroń, A. Kalinka, Properties of TiC and TiN reinforced alumina–zirconia composites sintered with spark plasma technique, Metals. 9 (2019) 1220. https://doi.org/10.3390/met9111220

[24] C.S. Kumar, S.K. Patel, Effect of WEDM surface texturing on Al_2O_3/TiCN composite ceramic tools in dry cutting of hardened steel, Ceram. Int. 44 (2018) 2510–2523. https://doi.org/10.1016/j.ceramint.2017.10.236

[25] P. Huber, D. Manova, S. Mändl, B. Rauschenbach, Formation of TiN, TiC and TiCN by

metal plasma immersion ion implantation and deposition, Surf. Coat. Tech. 174-175 (2003) 1243–1247. https://doi.org/10.1016/S0257-8972(03)00458-4

[26] M.A. Jaswon, R.D. Bhargava, Two-dimensional elastic inclusion problems, Math. Proc. Cambridge. 57 (1961) 669-680. https://doi.org/10.1017/S0305004100035702

[27] M. Gassner, N. Schalk, M. Tkadletz, C. Czettl, C. Mitterer, Thermal crack network on CVD TiCN/α-Al_2O_3 coated cemented carbide cutting tools, Int. J. Refract. Met. H. 81 (2019) 1–6. https://doi.org/10.1016/j.ijrmhm.2019.02.006

[28] M. Taya, S. Hayashi, A.S. Kobayashi, H.S. Yoon, Toughening of a particulate-reinforced ceramic-matrix composite by thermal residual stress, J. Am. Ceram. Soc. 73 (1990) 1382-1391. https://doi.org/10.1111/j.1151-2916.1990.tb05209.x

[29] M. Tkadletz, J. Keckes, N. Schalk, I. Krajinovic, M. Burghammer, C. Czettl, C. Mitterer, Residual stress gradients in α-Al_2O_3 hard coatings determined by pencil-beam X-ray nanodiffraction: The influence of blasting media, Surf. Coat. Tech. 262 (2015) 134-140. https://doi.org/10.1016/j.surfcoat.2014.12.028

[30] C.A. Botero, E. Jiménez-Piqué, C. Baudín, N. Salán, L. Llanes, Nanoindentation of Al_2O_3/Al_2TiO_5 composites: Small-scale mechanical properties of Al_2TiO_5 as reinforcement phase, J. Eur. Ceram. Soc. 32 (2012) 3723-3731. https://doi.org/10.1016/j.jeurceramsoc.2012.05.034

[31] V. Buscaglia, P. Nanni, Decomposition of Al_2TiO_5 and $Al_{2(1-x)}Mg_xTi_{(1+x)}O_5$ ceramics, J. Am. Ceram. Soc. 81 (1998) 2645-2653. https://doi.org/10.1111/j.1151-2916.1998.tb02672.x

[32] J.C. Caicedo, C. Amaya, L. Yate, M.E. Gómez, G. Zambrano, J. Alvarado-Rivera, J. Muñoz-Saldaña, P. Prieto, TiCN/TiNbCN multilayer coatings with enhanced mechanical properties, Appl. Surf. Sci. 256 (2010) 5898-5904. https://doi.org/10.1016/j.apsusc.2010.03.071